DETAILED X-RAY OBSERVATIONS OF THE CYGNUS LOOP

W. H.-M. Ku, K. Long, R. Pisarski, and M. Vartanian
Columbia Astrophysics Laboratory, Columbia University

ABSTRACT

High quality X-ray spectral and imaging observations of the
Cygnus Loop have been obtained with three different instruments. The
High Resolution Imager (HRI) on the Einstein Observatory was used to
obtain arcsecond resolution images of select bright regions in the
Cygnus Loop which permit detailed comparisons between the X-ray,
optical, and radio structure of the Loop. The Imaging Proportional
Counter (IPC) on the Einstein Observatory was used to obtain an
arcminute resolution map of essentially the full Loop structure.
Finally, an Imaging Gas Scintillation Proportional Counter (IGSPC),
carried aloft by a sounding rocket last fall, obtained modest resolu-
tion, spatially resolved spectrophotometry of the Cygnus Loop. An X-
ray map of the Loop in the energy of the O VIII line was obtained.
These data combine to yield a very powerful probe of the abundance,
temperature, and density distribution of material in the supernova
remnant, and in the interstellar medium.

1. INTRODUCTION

The Cygnus Loop is one of the most well-studied supernova rem-
nants (SNR) in our galaxy. Its close distance (770 pc) and large
size (~3°) make the Cygnus Loop an ideal candidate for detailed stu-
dies. Observations a decade ago by Gorenstein et al. (1971), and
Stevens and Garmire (1973) showed that the remnant was a copious
source of subkilovolt X-rays whose spectrum was consistent with ther-
mal emission from a thin hot plasma at a temperature of 3 million
degrees. These observations also suggested the presence of oxygen
line emission near 0.6 keV. A high resolution search with a Bragg
crystal spectrometer (Stark and Culhane 1978) led to only an upper
limit on the O VIII emission of 6% of the total X-ray flux. More
recently Inoue et al. (1980) and Kahn et al. (1980) presented new
evidence for the presence of oxygen line emission from the Cygnus
Loop. These data, in addition to the detection of 5303 Å Fe XIV
coronal line by Woodgate et al. 1974 constitute strong evidence for
the presence of hot plasma.

The spatial structure of the Cygnus Loop has been mapped by
several one-dimensional imaging systems (e.g., Stevens and Garmire

253

1973, Rappaport et al. 1974), and small aperature two-dimensional nonimaging detectors (Charles et al. 1975, Gronenschild et al. 1976) and has been found to be consistent in size with the 3° optical diameter of the remnant. The first true two-dimensional X-ray image of the Cygnus Loop was obtained by Rappaport et al. (1979) with a multi-wire proportional counter (MWPC) at the focal plane of a grazing incidence telescope on a sounding rocket. Their picture suggests that the X-ray emission arises from a limb-brightened shell of hot gas which resulted from the expansion of a blast wave into an inhomogenous interstellar medium (ISM). Unfortunately their observation had only limited useful spectral information (Kayat et al. 1981).

2. INSTRUMENT AND OBSERVATIONS

We describe here observations of the Cygnus Loop made with three different X-ray imaging systems over the past three years: (1) An imaging gas scintillation proportional counter (IGSPC) with solid state spectrometer-type spectral resolution below a 1 keV and 12' spatial resolution carried aloft by a sounding rocket; (2) An imaging proportional counter (IPC) with modest spectral resolution (100% @ 1.5 keV) and 1'-2' spatial resolution operated on the Einstein Observatory; (3) A microchannel plate (HRI) with no spectral information but 4" spatial resolution operated on the Einstein Observatory. Table 1 summarizes the properties of the three instruments at 654 eV.

TABLE 1
Instrument Parameters

Instruments	F.O.V.	(Performance @ 654 eV)		
		$\Delta E(eV)$ (FWHM)	ΔS (FWHM)	B $c/ks/(mm)^2$
IGSPC/Rocket	150'	177	~12'	0.06
IPC/Einstein	60'	~1000	2'	0.5
HRI/Einstein	25'	------	4"	4.0

A Nike boosted Black Brant sounding rocket carrying an IGSPC at the focal plane of a grazing incidence telescope was launched on 17 November, 1981. The rocket pointed at the W limb of the Cygnus Loop and then scanned over to the NE limb- holding at each position for 120 s. Fig. 1 shows a copy of a POSS picture of the Cygnus Loop overlaid with the circular field of view of the IGSPC. The positions of the millimeter wide window support ribs relative to the centers of the two IGSPC pointings are sketched.

Fig. 2 shows a merged image of the two pointings corrected for exposure but uncorrected for ribs and vignetting. The log intensity scale in arbitrary units is shown to the right. The spatial scale is

shown on the bottom. Large scale X-ray features observed by several groups prior to Einstein are clearly seen in Fig. 2. The bright NE, N, and W limbs are seen corresponding roughly to similar bright features in the optical and radio regimes.
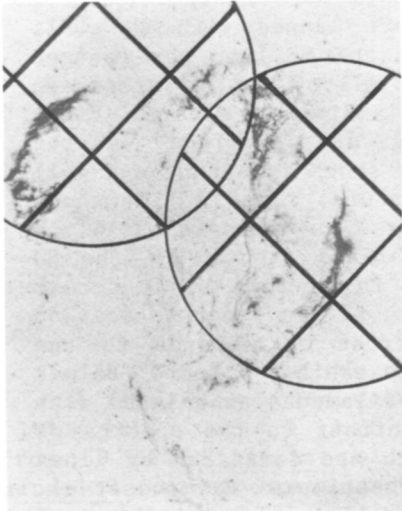

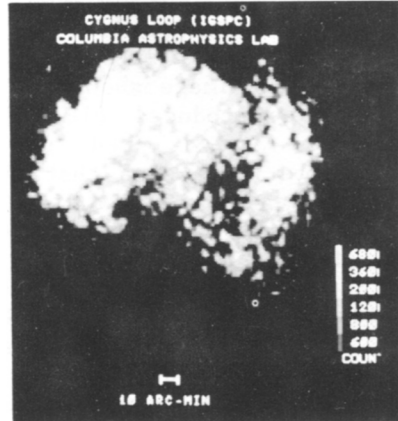Fig. 1 – Overlay of the 150' IGSPC field of view on the POSS print of the Cygnus Loop.

Fig. 2 – The total spatial data from the two IGSPC pointings have been combined to form one image.

An arcminute resolution image of the total 0.1-4.5 keV X-ray emission observed by the IPC is plotted on top of a POSS print in Fig. 3. The composite image is formed by merging the central 35' x 35' region of 59 overlapping IPC fields (one field near center north is missing). Over all, the X-ray bright shell demonstrates remarkable symmetry after 18,000 years of expansion. The X-ray emission is centered on R.A. (1950.0) = $20^h49^m15^s$ and Dec (1950.0) = 30°51'30", with a radius of 84'. Except for the breakout near the south (away from the galactic plane), the shell is circular to within ±5'. The contrast seen is very high with the brightest feature on the NE and W limb ~300 times brighter than the diffuse X-ray background and ~100 times brighter than the faintest region within the circular shell. Faint X-ray emission (≲1000 times the peak surface brightness) extends beyond the shell on the W and SW and extends ~25' beyond the bottom of this image (to δ = 28° 30'). Radial surface brightness profiles confirm this and also reveal considerable (>3:1) limb brightening – favoring the presence of adiabatic (rather than isothermal) blast waves (Solinger, Rappaport, and Buff 1975). IPC images formed in several different energy bands were examined and found to be extremely similar in general outline although, as we shall see later, spectral variations across the remnant do exist. Two point sources, ~ 10^{-3} times the total intensity of the Loop, are observed within the X-ray shell at α = $20^h46^m24^s$, δ = 31°31'43" and α

= $20^h43^m35^s$, δ = 30°32'20". Eleven other point sources- stars or
active galaxies- are seen just outside the shell. No point sources
are visible near the center of the remnant although enhanced emission
is seen 7' to the NW and NE of the center near enhanced optical emis-
sion. Any neutron star remnant must be colder than 9×10^5 K.

The brightest regions of the loop were mapped with the HRI.
Five pointings on the W limb and twelve on the NE limb were merged
together to form the image shown in Fig. 4. All of the features seen
in the IPC are reproduced clearly. In addition, several finer
features may be noted when the images are examined on the
subarcminute scale. One sees that while the shock is strong and well
defined in some regions, it is diffuse in others. The NE limb shows
a bright ~8' wide barlike feature with excess X-ray emission 3'-4' in
front ending in a fainter but still well-defined front. On the SW
limb, a very strong bow-shaped shock front is seen. A break across
the main shock front with a new shock forming ~5' in front is seen on
the W limb. The position of this new front corresponds to the
location of a faint optical filament found to exhibit a "pure" Balmer
spectrum, similar to the spectra of optical filaments associated with
the much younger Tycho SNR and in sharp contrast to the spectra of
the bright optical filaments in Cygnus which are dominated by lines
of [OIII]. Our observations support the suggestion of Raymond et al.
(1980) that these lines result from the collisional excitation of
cold ISM material swept up by a fast shock. The close
identification of this X-ray feature with the optical filament is
repeated for the Hβ + Hα + [NII] filament noted by Gull et al.
(1977) on the northern boundary of the Loop and the nonradiative
shock outside the NE limb studied by Raymond (this volume). Other
optically bright filaments are seen to
correspond to regions of enhanced X-ray emission in general but not
in detail. For example the bow shaped shock front has no bright
optical counterpart, while a bright optical filament on the NE limb
actually extends past the boundary of the X-ray emission. The
identification of X-ray features with radio emission is also gene-
rally good but poor in detail. We have compared the X-ray emission
with the 2.7 GHz map of Keen et al. (1974). The X-ray and optically
bright NE and W limb are seen clearly in the radio. Faint radio
emission is seen all around ~5' inside the X-ray emission except in
the SE quadrant. Weak radio emission is seen outside the W limb
similar to the optical and X-ray images. In the S and SW, the
breakout is seen more strongly in the radio than in the X-ray. The E
edge of the breakout is strong in all bands while the W edge is only
strong in the radio.

While the HRI provides the greatest detail on the spatial struc-
ture of the Cygnus Loop, it has no spectral information. The IPC has
some spectral capabilities which are just now being exploited. Tem-
poral and spatial variations in the IPC detector gain have hampered
the analysis of the pulse height information for most sources. How-
ever the Cygnus Loop IPC observations benefit from several features
which improve the reliability of the spectral parameter estima-

Fig. 3 - The central 35' × 35', 0.1-4.5 keV data from 59 IPC Einstein pointings merged in an exposure corrected manner and overlaid on a POSS image of the Cygnus Loop. Contours are set at equal log intervals (0.3).
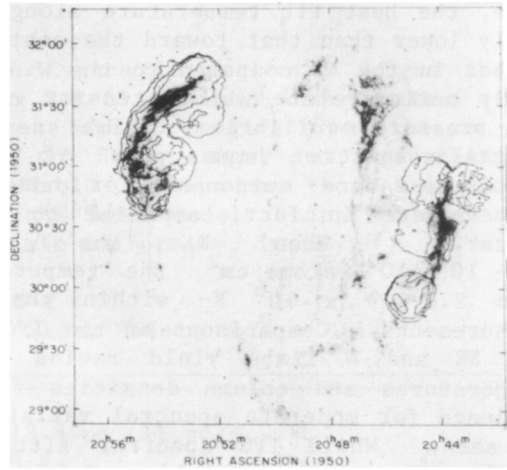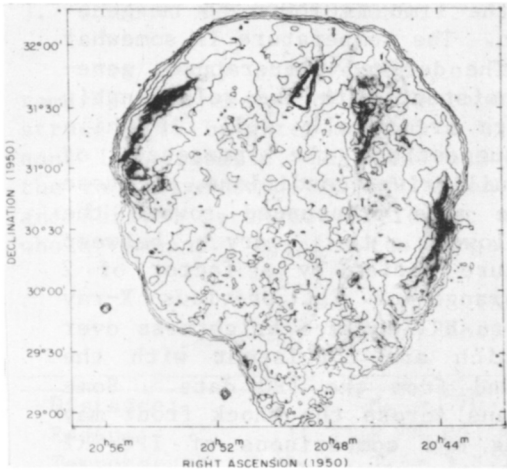
Fig. 4 - The central 25' diameter data from 19 HRI Einstein pointings merged in an exposure corrected manner and overlaid on a POSS image of the Cygnus Loop. Contours are set at equal log intervals (0.3).

tions. 1) Because of the considerable overlap among observations, we can limit ourselves in most cases to examining the central IPC regions where the IPC's response is better mapped; for interesting off-axis regions (>20') we can check the spectra obtained in ≥ 2 pointings against one another. 2) Because the observations were often done alternately inside and outside the shell at near coincident time with similar gain and background conditions, we can use the outside fields for background subtraction. Using 6' radius cells, we summed all the IPC counts in a source image, subtracted the exposed normalized counts from the same counter region in a background field and fitted the spectra to a Raymond and Smith (1979) model with cosmic abundances. Both N_H the hydrogen column density and T the plasma temperature, were allowed to vary although due to the poor resolution of the IPC at low energies and the strong anticorrelation between N_H and T there is little leverage on the N_H parameter so we limited its variation to $1 - 10 \times 10^{20}$ atoms cm^{-2} (accomodating all X-ray values, and E(B-V) $\simeq 0.05 - 0.15$ $(2 - 8 \times 10^{20})$ reddening measurements (Raymond et al. 1981)). We also added an estimated 5% residual systematic error to the data before minimizing χ^2 measures of the fit of models to the data. A typical fit to the data is shown in Fig. 5. Most of the flux at the best fit temperature of 2.1×10^6 K is due to line emission from OVII, OVIII, NVI, NVII, and CVI with contributions from FeXVII. To simplify the interpretation of possible spectral gradients, we fixed log N_H at 20.6. When this was

done, the best fit temperature along the limb is found to be gene-
rally lower than that toward the center. The temperature is somewhat
higher in the NE compared to the W. The derived temperatures gene-
rally anticorrelate with intensity consistent with the relationship
for pressure equilibrium. Limb spectra are usually well fit while
central spectra have poor χ^2 suggesting the presence of
multitemperature components or nonequilibrium conditions. These
effects are in fact, expected to be more pronounced toward the
center. When N_H was allowed to vary between
$1 - 10 \times 10^{20}$ atoms cm^2 the temperature varied by a factor of 2
from 2.0–4.3 x 10^6 K- within the range of all previous X-ray
measurements. Comparisons of the IPC to HRI surface brightness over
the NE and W limbs yield ratios which are consistent with the
temperatures and column densities found from the IPC data. Some
evidence for moderate spectral variations across the shock front may
be seen. While IPC spectral fitting and comparisons of IPC/HRI
brightness ratios can yield useful estimates of the temperature vari-
ation across the remnant they do not permit detailed studies of the
distribution of temperature, density, and abundance gradients in the
Loop. The IGSPC provides better diagnostics. Fig. 6 shows the total
spectrum obtained by the IGSPC for the NE limb. The measured spec-
trum is markedly different from that obtained by the IPC and reflects
the presence of absorption near 0.28 keV by the carbon in the 2μ
polypropylene window used (unresolved by the IPC), line emission from
oxygen near 0.65 keV, and mirror cutoff above 1.5 keV. The fit (his-
togram) does not include detailed postflight calibration done re-
cently at MSFC and is therefore preliminary. Nevertheless a
2×10^6 K plasma with cosmic abundance and log N_H = 20.65 reproduces
the general features of the spectrum quite well. The presence of
line emission near 0.65 keV is absolutely required to fit the data.
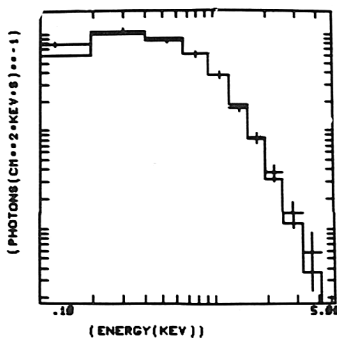The W limb shows qualitatively the same features.

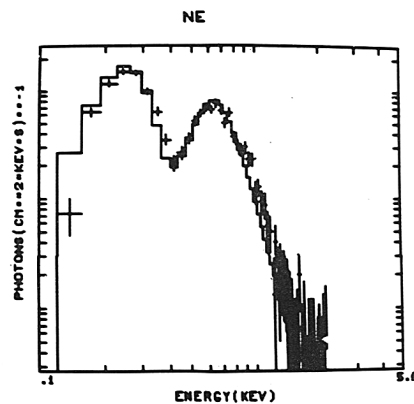Fig. 5 – Typical IPC pulse height spectrum of photons collected in 12' diameter circle centered on α = 20^{h}44^{m}10^s, δ = 29°41'.

Fig. 6 – Typical IGSPC pulse height spectrum of photons collected in 150' diameter circle centered on α = 20^{h}52^{m}10^s, δ = 31°50'.

3. SUMMARY AND CONCLUSIONS

New X-ray observations of the Cygnus Loop clearly reveal the remarkable symmetry of the expanding SNR blast wave. Observations of strong limb brightening and a hotter interior suggest that the remnant is adiabatic, near the end of the Sedov stage, and approaching the radiative stage of evolution. Table 2 summarizes those measured and derived parameters relevant to the Sedov model as applied to the whole remnant. Despite the large scale uniformity, it is

TABLE 2
Cygnus Loop: Sedov Model

Distance:	$d = 770$ pc
Radius:	$R_x = 84' = 18.8$ pc (± 1 pc)
Temperature:	$T_x = 3 \times 10^6$ K
Limb temperature:	$T_s = 2 \times 10^6$ K
X-ray luminosity	$L_x = 9 \times 10^{35}$ ergs s^{-1} (0.1-4.0 keV)
ISM density:	$N_H = 4 \times 10^{20}$ atoms cm^{-2}; $n_H = 0.16$ cm^{-3}
Shock velocity:	$V_s = 400$ km s^{-1}
Initial SN energy:	$E_0 = 3 \times 10^{50}$ ergs
Age:	$t = 18,000$ yrs
Total mass:	$M = 100$ M$_\odot$

also clear that a range of different temperatures, densities, and abundances apply to different regions of the remnant. We believe these differences reflect differences in the ISM. The Cygnus Loop probably sits in a low density 0.1 cm^{-3}, warm ~10^4 K ISM. This ISM contains many cold $\lesssim 10^3$ K , ~1-10 pc clouds with densities $\gtrsim 10$ cm^{-3} which have been shocked by the blast wave. The compressed gas and magnetic field yield the radio synchrotron emission. Material heated and compressed by the passing shock cool and radiate in the optical. The general coincidence of X-ray, optical, and radio peaks suggest that evaporative heating of these clouds in the hot postshock region may be occurring. The breakout in the south may reflect the shock front encountering a hot, $\gtrsim 10^5$ K low density $\lesssim 0.01$ cm^{-3}, ~10 pc "tunnel" in the ISM. Further work on detailed studies of the temperature and density variations in the Loop and detailed comparisons between X-ray, optical, and radio fine structure may clarify the structure of the ISM.

However, it is already clear from these data that X-ray observations can provide an extremely detailed look at the ISM. In particular, spatially resolved spectrophotometry with the IGSPC on AXAF should provide an excellent diagnostic of the SN shock and the ISM.

4. REFERENCES

Charles, P. A., Culhane, J. L., Zarnecki, J. C. 1975, *Astrophys. J.*
  (Letters), 196, p. L19.
Gorenstein, P., Harris, B., Gursky, H., Giacconi, R., Novick, R., and
  Van den Bout, P. 1971, *Science*, 172, p. 369.
Gronenschild, E.H.B.M., Mewe, R., Heise, J., Brinkman, A. C.,
  den Boggende, A.J.F., and Schrijver, J. 1976,
  Astron. Astrophys. 49, p. 153.
Gull, T. R., Parker, R.A.R., and Kirschner, R.P. 1977, in
  Supernovae, ed. D. N. Schramm (Dordrecht: Reidel), p. 71.
Inoue, H., Koyama, K., Matsuoka, M., Ohashi, T., Tanaka, Y., and
  Tsunemi, H. 1980, *Astrophys. J.*, 238, p. 886.
Kahn, S.M., Charles, P.A., Bowyer, S., and Blissett, R.J. 1980,
  Astrophys. J., 242, p. L19.
Kayat, M.A., Rolf, D.P., Smith, G.C., and Willingale, R. 1980,
  Mon. Not. R. Astro. Soc., 191, 729-737
Keen, N.H., Wilson, W.E., Haslam, C.G.T., Graham, D.A., and
  Thomasson, P. 1973, *Astron. Astrophys.*, 28, p. 197.
Rappaport, S., Doxsey, R., Solinger, A., Borken, R. 1974,
  Astrophys. J., 194, p. 329.
Rappaport, S., Petre, R., Kayat, M. A., Evans, K. D., Smith, G. C.,
  and Levine, A. 1979, *Astrophys. J.*, 227, p. 285.
Raymond, J. C. and Smith, B. W. 1977, *Astrophys. J. Suppl.*, 35, 419.
Raymond, J. C., Davis, M., Gull, T. R., and Parker, R.A.R. 1980,
  Astrophys. J., 238, p. L21.
Solinger, A., Rappaport, S., and Buff, J. 1975, *Astrophys. J.*, 201,
  p. 381.
Stark, J.P.W., and Culhane, J. L. 1978, *Mon. Not. R. Astr. Soc.*,
  184, 509.
Stevens, J. C., and Garmire, G. P. 1973, *Astrophys. J. (Letters)*,
  180, L19.
Weisskopf, M. C., Helava, H., and Wolff, R. S. 1974, *Astrophys. J.*
  (Letters), 194, L71.
Woodgate, B. E., Stockman, H. S., Angel, J.R.P., and Kirschner, R. P.
  1974, *Astrophys. J. (Letters)*, 188, L79.